https://doi.org/10.5194/wes-2026-13
Preprint. Discussion started: 26 January 2026

WIND ENERGY SCIENCE DISCUSSIONS

Impact of Wake Impingement on the Fatigue Loads in the Main Bearings and Blades of Offshore Wind Turbines

Jakob Gebel[1,2], Pieter-Jan Daems[2], Diederik van Binsbergen[1,2], Veronica Liverud Krathe[1], Amir R. Nejad[1], and Jan Helsen[2,3]

[1]Department of Marine Technology – Norwegian University of Science and Technology (NTNU), Trondheim, Norway
[2]Department of Mechanical Engineering – Vrije Universiteit Brussel (VUB), Brussels, Belgium
[3]FlandersMake@VUB, Brussels, Belgium

Correspondence: Jakob Gebel (jakob.gebel@ntnu.no)

Abstract.

This study investigates the impact of wake impingement on the fatigue loads in the components of offshore wind turbines. More specifically, the focus of this paper lies on the blades and the main bearings of a geared wind turbine. For this, OpenFAST models of a deployed 8.4 MW turbine are coupled in the mid-fidelity wind farm simulation tool FAST.Farm, to simulate load time series of turbines operating under wake interactions. A two-step analysis is carried out: first, a parametric study explores the influence of turbine spacing and wake overlap on fatigue loads; second, a case study applies the framework to a real offshore wind farm in the Belgian North Sea. Results show that wake interactions can reduce blade root loading at below-rated wind speeds but significantly increase fatigue damage above rated conditions, while main bearing lifetimes exhibit strong asymmetries depending on the side of wake impingement. The farm-level analysis highlights spatial variability in component degradation, showcasing how damage maps can be obtained that link turbine position, inflow direction, and operating conditions to expected lifetime reductions. These findings underline the importance of considering wake effects in design, lifetime assessment, and operation and maintenance planning of offshore wind farms.

1 Introduction

When a turbine extracts energy from the wind, it generates a region of reduced velocity (velocity deficit) and increased turbulence behind it, known as the wake (Porté-Agel et al., 2019; Meyers et al., 2022). Turbines located downstream of other turbines operate within this wake, which affects their performance and loading (Fleming et al., 2014; Damiani et al., 2018; Bossanyi, 2018; Binsbergen et al., 2020; Thedin et al., 2024). As a result, turbines that frequently experience wake impingement may degrade differently than those in the front row relative to the prevailing wind direction.

With the increasing size and number of offshore wind farms, the influence of wake effects on turbine performance and lifetime has become an important area of research. While the impact on power production has been extensively studied (Fleming et al., 2014; Damiani et al., 2018; Bossanyi, 2018; Binsbergen et al., 2020; Thedin et al., 2024; Kecskemety and McNamara, 2011; Barthelmie et al., 2010; Tang et al., 2019), the consequences for fatigue loads and component lifetime remain less well understood. Recent studies addressing this gap include:

Quick et al. (2025), who performed a parametric analysis using a 10MW turbine in OpenFAST, showed that partial wake impingement can reduce the rating life of the axially supporting main bearing by up to 73.5% for the rotor-side bearing and 96.7% for the generator-side bearing under otherwise identical conditions. The study showed that fatigue damage depends on which side of the rotor is exposed to the wake. In addition, a full wind farm layout analysis revealed that main bearing fatigue life is reduced by up to 25% for turbines within the farm, when considering all operational wind speeds and their occurrences during the operational lifetime.

Krathe et al. (2025) investigated the main bearing response on a floating 15MW wind turbine subjected to wakes. They focused on below-rated wind speeds and represented neutral, stable, and unstable atmospheric conditions through Large Eddy Simulations to investigate their effect on downstream wake effects. They found that these atmospheric conditions and the extent of wake overlap heavily influence fatigue damage.

Building on prior studies showing that wake impingement can substantially reduce main bearing rating life, this study assesses wake-induced fatigue loads in an operating offshore wind farm using a site-specific turbine model, layout, and historical wind conditions. It further extends the assessment to blade-root fatigue for cross-component comparison, and relates fatigue loads to energy production.

The present study investigates how relative turbine positions and resulting wake effects influence fatigue loads and focuses particularly on partial wake overlap and the resulting asymmetric rotor-plane loading, which have been shown to impact component fatigue life significantly (Quick et al., 2025; Krathe et al., 2025). In addition, the study explores the effect of turbine spacing, providing insight into the sensitivity of fatigue damage to inter-turbine distance within wind farm layouts. Turbine spacing is a crucial parameter in the design of new wind farms layouts, as power density must be weighted against wake effects.

The wind turbine components considered in this work include the main bearings and the blades. These components are specifically chosen based on their relevance to turbine downtime, maintenance effort and their environmental footprint (Keller et al., 2016; Hart et al., 2020; Mishnaevsky, 2022; Katsaprakakis et al., 2021; Liu and Barlow, 2017). Similar to the study by Quick et al. (2025), a two-stage methodology is employed. First, a parametric study is conducted using two turbines to assess the effects of wake impingement on fatigue damage under controlled conditions, systematically varying the relative turbine positions and wind speeds. Here, the study provides a detailed assessment of the asymmetric main bearing fatigue loading under waked inflow conditions; second, a full wind farm layout is analysed to reveal differences in component degradation stemming from a turbines' locations within the wind farm. The goal of the full farm simulation is to deliver an exemplary damage map that shows how the degradation rate for a component changes with the inflow direction, such that fatigue damage estimations can be obtained quickly based on inflow conditions, without the necessity to perform new simulations. The analysed wind turbines represent deployed wind turbines of a farm in the Belgian North Sea. The study contributes to a better understanding of spatial variability in turbine lifetimes and provides insights for lifetime-aware operation and maintenance as well as wind farm design. Novelty lies in utilising a model of a deployed turbine, together with the layout and meteorological data from an existing wind farm, to obtain fatigue metrics for decision support, and in the extended discussion of asymmetries in main bearing loading.

https://doi.org/10.5194/wes-2026-13
Preprint. Discussion started: 26 January 2026

The paper is structured as follows: First, the necessary simulation framework is introduced (Section 2.1) and the applied fatigue damage calculation methods are described (Section 2.2). To facilitate readability, the two studies are then discussed sequentially. The parameteric two-turbine study is described, and its results are discussed (Section 3), followed by the full wind farm case study and its corresponding findings (Section 4). In the end, conclusions are drawn, and future steps are outlined (Section 5).

2 Methodology

The basis of this work is provided by a simulation setup that uses individual wind turbine models (Section 2.1.1), which are coupled within a shared computational domain (Section 2.1.2). This framework provides the necessary load time series to calculate fatigue loads in main bearings and the blade roots (Section 2.2), while accounting for wake interactions of the turbines.

2.1 Simulation Framework

2.1.1 OpenFAST

The individual wind turbines are modeled using the aero-hydro-servo-elastic framework OpenFAST and represent an 8.4 MW bottom-fixed offshore wind turbine located in the Belgian North Sea. The model is derived from a scaled reference turbine using the installed turbine's design data and field measurements, as described in the authors' previous work (Gebel et al., 2025b). The model was calibrated using identified modal behavior and observed operational performance obtained from drivetrain vibration measurements and SCADA data. For the turbine control, the ROSCO controller (Abbas et al., 2022) was implemented and tuned to follow power, pitch, and RPM curves from SCADA data to replicate the turbine's control behavior. In addition to operational values such as power output, rotor speed, and pitch angle, the model can generate load time series at multiple locations of the turbine (e.g. hub, blade root, and tower bottom), as well as a wide range of other structural and aerodynamic responses depending on the analysis objectives.

2.1.2 FAST.Farm

To model the aerodynamic interactions between wind turbines, this work employs FAST.Farm, a mid-fidelity, time-domain simulation tool developed as an extension of OpenFAST. FAST.Farm enables coupling of multiple OpenFAST turbine models and captures key wake characteristics, such as wake deficit, wake meandering, wake-added turbulence, and wake merging, under varying atmospheric conditions, using the Dynamic Wake Meandering model (Larsen et al., 2007). To capture the flow and the aerodynamic interactions, FAST.Farm uses a shared simulation domain for all simulated wind turbines, discretised into grid points where the flow conditions are calculated. To reduce calculation time, the domain uses a global coarse grid and locally refined grids around the turbines, as depicted in Figure 2 found in Section 3. The domain dimensions and discretisation parameters for the parametric study and the case study follow the modelling guidelines provided by NREL (OpenFAST

Development Team, 2024) and are listed in Table 1. In this context, DT_Low and DT_High denote the timesteps for the coarse and fine grids, while DS_Low and DS_High specify the corresponding spatial resolution.

Table 1. FAST.Farm domain discretisation

Case	DT_Low [s]	DT_High [s]	DS_Low [m]	DS_High [m]	Low resolution box size [m]	High resolution box size [m]
Two turbines	1	0.1	10	5	2410 × 1480 × 360	360 × 360 × 360
Full farm	1	0.1	10	5	10000 × 10000 × 360	360 × 360 × 360

The wind fields for all simulations are generated with HiperSim employing Mann turbulence boxes and 3D frozen turbulence fields (Dimitrov et al., 2024). The atmospheric conditions are not varied between the simulated cases: the turbulence follows the class C normal turbulence model from IEC 61400-1 (2019), and the wind shear exponent is 0.14.

2.2 Fatigue damage calculation

2.2.1 Blades

To assess fatigue loads in the blades, the blade roots are examined, as this is the location with the highest bending moments along the blade. The fatigue failure of wind turbine blades results from an accumulation of damage due to cyclic loading, and its analysis is specified in IEC 61400-1 (2019) and IEC 61400-5 (2019). To compare the effect of different load time series, the damage equivalent load (DEL) is commonly used as a metric. The DEL condenses the load time series into a single equivalent load that causes the same fatigue damage as the actual variable loads for a set number of reference cycles. The DEL builds on the idea of linear damage accumulation and is expressed as (Thomsen, 1998):

$$\mathrm{DEL} = \left(\sum \frac{n_\mathrm{i}\, S_\mathrm{i}^m}{N_\mathrm{Ref}} \right)^{\frac{1}{m}} \tag{1}$$

where n_i denotes the number of cycles in each load range S_i obtained through rainflow counting. The DEL is set to act with a frequency of 1 Hz , which determines the number of reference cycles $N_{Ref} = 600$, for the 10-minute time series. The Wöhler exponent, m, is chosen as 10 for the composite material of wind turbine blades (Freebury and Musial, 2000; Schmidt et al., 2025). The load ranges for the blade root are based on the resultant moment of the flapwise and edgewise bending moments at the root of one blade, which are directly obtained from OpenFAST.

2.2.2 Main bearings

Main bearings are fully rotating bearings whose design lifetime is expressed in terms of the basic rating life, L_{10}. Defined in the ISO 281 (2007), the basic rating life L_{10} denotes the number of revolutions (in millions) that a bearing can be expected to endure with 90% reliability under constant loading. This metric provides the reference for the bearing fatigue and is defined as:

$$L_{10} = \left(\frac{C}{P}\right)^{a} \tag{2}$$

where, C is the basic dynamic load rating of the bearing, the exponent a is $10/3$ for roller bearings, and P is the equivalent dynamic bearing load, a hypothetical load, constant in magnitude and direction, which, when applied, has the same influence on bearing life as the axial and radial loads to which the bearing is subjected. The equivalent dynamic bearing load is calculated as:

$$P = XF_r + YF_a \tag{3}$$

where F_r and F_a are the radial and axial bearing loads, defined as $F_r = \sqrt{F_y^2 + F_z^2}$ and $F_a = F_x$. The load factors X, Y, and the axial-to-radial load ratio e are shown in Table 2.

For a time-varying loading, P can be calculated for each timestep of the load time series to obtain an equivalent steady load P_{eq} with (Shigley, 2011):

$$P_{eq} = \left(\frac{\sum n_{\mathrm{i}} P_{\mathrm{i}}^{a}}{\sum n_{\mathrm{i}}}\right)^{\frac{1}{a}} \tag{4}$$

where n_{i} denotes the number of rotations of the main shaft during a timestep i, obtained from its rotational speed w_{i} (rpm) and the timestep length t_{i} as $n_{\mathrm{i}} = \frac{w_{\mathrm{i}}}{60} t_{\mathrm{i}}$. The equivalent dynamic load P_{i} for each timestep is calculated according to Equation 3.

P_{eq} can be directly used in Equation 2 to obtain L_{10}, as the number of revolutions the bearing is expected to endure under loading equivalent to the given load time series. This makes P_{eq} a suitable metric for comparing the fatigue loads of the main bearings, ensuring consistency with the DEL, since both are expressed as loads (Nejad et al., 2017).

Due to confidentiality, there is limited information available for the main bearings of the deployed offshore wind turbine. As advised by the bearing manufacturer SKF, the bearing arrangement is assumed to have an upwind non-locating compact aligning roller bearing (CARB) and a downwind locating double-row spherical roller bearing (SRB). This arrangement provides a more balanced load distribution than a configuration with an upwind-locating and a downwind non-locating bearing. Following this, a SKF 249/1320 CAF/W33 was chosen as the locating bearing while a C 30/950 MB was chosen as the non-locating bearing from available bearing catalogues (Schaeffler Technologies AG & Co. KG, 2016; SKF Group, 2018). The relevant bearing parameters for the fatigue load calculation are given in Table 2.

As the drivetrain is modelled as a simple two-mass-spring and damper system in OpenFAST, the necessary reaction forces at the main bearings (F_x, F_y, F_z) are not directly obtained from the turbine model. Instead, an analytical model is used to calculate the bearing loads based on the simulated hub loads from OpenFAST. Adopted from Krathe et al. (2025), the main shaft is treated as a supported beam with the main bearings as its supports (Figure 1).

Table 2. Bearing parameters for calculation of L_{10}

Bearing	$\frac{F_a}{F_r} \leq e$		$\frac{F_a}{F_r} > e$		e	C [MN]
	X	Y	X	Y		
MB1 (CARB)	1	0	NA	NA	0.16	13.2
MB2 (SRB)	1	3.2	0.67	4.8	0.21	18.7

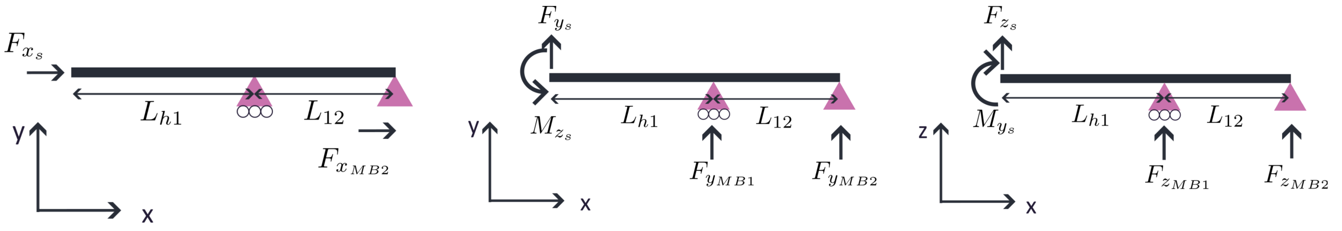

(a) Forces along local x.

(b) Loads in local yx-plane.

(c) Loads in local zx-plane.

Figure 1. Analytical load diagram of the shaft loads in the local coordinate system, adopted from Krathe et al. (2025).

Assuming that the main bearings carry all non-torque loads, the reaction forces at the bearings can be determined directly from the forces (F_{i_s}) and moments (M_{i_s}) acting at the shaft tip. These loads include aerodynamic forces as well as those resulting from rotor mass and inertia. With the bearings treated as rigid supports, the vertical forces can be calculated as follows:

$$F_{z,\text{MB1}} = \frac{M_{y,s} + F_{z,s}(L_{h1} + L_{12})}{L_{12}} \tag{5}$$

$$F_{z,\text{MB2}} = \frac{-M_{y,s} - F_{z,s}L_{h1}}{L_{12}} \tag{6}$$

While the lateral forces on the bearings are calculated with:

$$F_{y,\text{MB1}} = \frac{M_{z,s} + F_{y,s}(L_{h1} + L_{12})}{L_{12}} \tag{7}$$

$$F_{y,\text{MB2}} = \frac{M_{z,s} - F_{y,s}L_{h1}}{L_{12}} \tag{8}$$

https://doi.org/10.5194/wes-2026-13
Preprint. Discussion started: 26 January 2026

The axial loads are only taken by the locating bearing and calculated with:

$$F_{x,\mathrm{MB2}} = F_{x,s} \tag{9}$$

Compared to the equations from Krathe et al. (2025), one will find the gravity loads from the generator rotor mass (m_{gr}) and its inertia (J_{gr}) to be omitted in here. Krathe et al. investigated a direct-drive system in which the generator rotor is directly connected to the main shaft, whereas the turbine considered in this work has a geared drivetrain. The necessary distances L_{h1} and L_{h12} were provided by the turbine operator but cannot be disclosed.

It should be noted that the applied damage metrics are not exhaustive, as they do not capture all possible failure modes. The L_{10} metric is commonly used in bearing sizing and reflects the rolling contact fatigue of the main bearings. In practice, however, many bearing failures may arise from different mechanisms that are more complex to model. Likewise, the DEL is used as a comparative measure of blade root loading. It must be emphasised that it cannot reflect all failure modes of the composite material, such as those resulting from local imperfections for example.

3 Parametric Study

The parametric study aims to evaluate how the fatigue loads of a wake-impinged turbine depend on the degree of wake overlap and on the turbine spacing. For this, two turbines are placed in the same domain, and their relative position is varied systematically by changing the cross-flow offset and the turbine spacing (Figure 2). The cross-flow offset, expressed in multiples of the rotor diameter (D), primarily influences wake overlap and is varied from –1.5D to 1.5D in 0.1D increments. The turbine spacing refers to the downstream distance between turbines, and four different distances are simulated: 3.5D, 5D, 7D, and 10D. This range is chosen based on observed turbine spacings of operational wind farms. Increasing the turbine spacing gives the wake more time to mix with the atmosphere, and the wake velocity deficit and turbulence intensity decrease over time and downstream distance. It is then investigated how the occurring loads on the machine are affected.

Since the generated wind fields exhibit local turbulence-induced differences, the downstream turbine remains fixed in position across all simulation cases, while the upstream turbine is repositioned to achieve different relative positions between the two turbines. To obtain a reference for the occurring loads without wake impingement, an additional simulation is carried out with only the downstream turbine present in the domain, subjected to the same wind field. The study is conducted at wind speeds of 8, 10, 12, 16, and 20 m/s, covering operation below, around, and above the rated wind speed. For each wind speed, the same turbulence field is used across simulations to ensure that differences in the results can be attributed solely to changes in cross-flow offset and downstream distance. An overview of the load cases is given in Table 3.

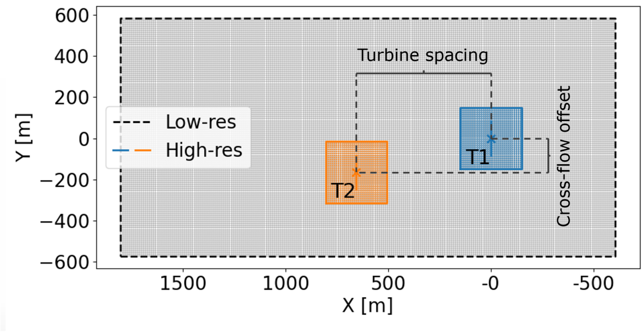

Figure 2. Setup of the simulation domain with high- and low-resolution regions and definition of cross-flow offset and downstream distance.

Table 3. Simulation parameters for the parametric study

Parameter	**Values**			
Turbine Spacing [in D]	3.5	5	7	10
Cross-flow Offset [in D]	-1.5 to 1.5 in 0.1 increments			
Windspeed [m/s]	8	10	12	20

3.1 Results for Blade Root Damage

The change in DEL at the blade root of the downstream turbine (T1) is shown in Figure 3a as a function of the relative position of the upstream turbine (T2). Previous studies (Gebel et al., 2025a) have shown that blade root DEL closely follows the thrust curve, with the highest values occurring near rated conditions. Thus, the observations are best distinguished between below-rated and above-rated wind speeds, with the rated wind speed being 11.4 m/s.

At below-rated wind speeds, wake-induced velocity deficits reduce the incoming wind speed and therefore the thrust, which leads to lower DEL at the blade root. This reduction becomes stronger the closer T2 is located, reaching up to 30% for the smallest turbine spacing at 8 m/s.

For above-rated wind speeds, the wake-induced velocity deficits have the opposite effect and lead to an increase in DEL. In this operating region, the thrust on the blades increases with decreasing wind speed, so the presence of the wake amplifies fatigue loading. This effect is more pronounced at 16 m/s than at 20 m/s, as the thrust curve has a steeper gradient around 16 m/s. At 16 m/s wind, the DEL increases by up to 10% relative to free-flow conditions at the minimal turbine spacing.

For 12 m/s, minimal turbine spacing does not result in an increase in DEL. The wake impingement at turbine spacings below 5D and small crossflow offsets reduces the wind speed to below 11.4 m/s, such that the peak thrust is passed and the acting thrust becomes similar to that under free-flow conditions. For all wind speeds, the wake effects become negligible when the cross-flow offset exceeds approximately $\pm 1.3D$.

Although wake impingement at below-rated wind speeds reduces component damage per unit time, it simultaneously lowers power production. Thus, the trade-off between lifetime and energy yield must be considered. Figure 3b presents the change in DEL normalised with the produced energy [MWh]. It becomes evident that wake effects result in higher DEL per unit of power, particularly at low wind speeds. Consequently, power production becomes less fatigue-efficient, meaning that the turbine accumulates more fatigue damage per generated MWh than under non-waked conditions.

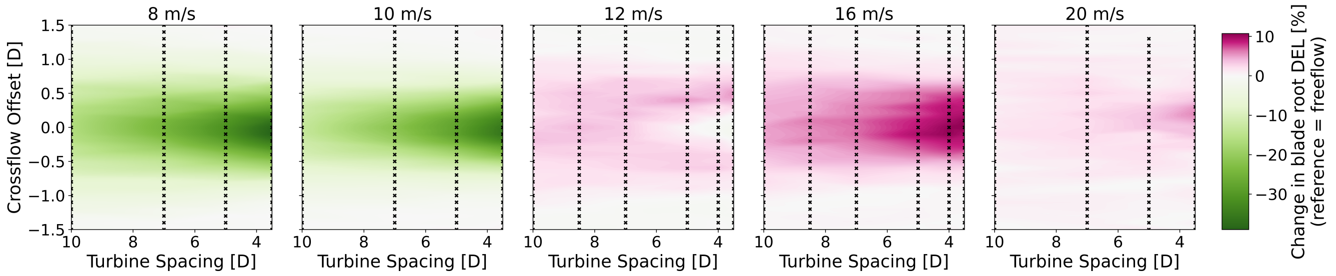

(a) Change of DEL w.r.t. free-flow

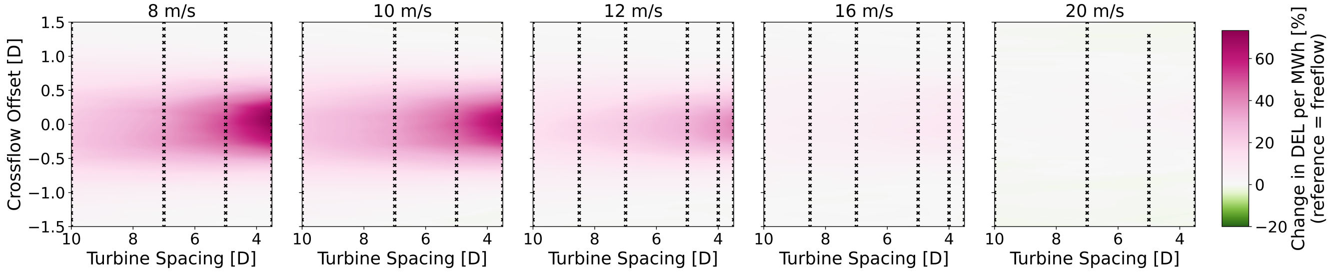

(b) Change of DEL per MWh of produced energy w.r.t. free-flow

Figure 3. Fatigue loads in the blade root of T1 as a function of the relative location of T2 for different wind speeds. The x-marks indicate parameter combinations for which simulations were carried out, based on which the colour map is interpolated.

3.2 Results for Main Bearing Lifetime

Figure 4 shows the P_{eq} of the main bearings of the downstream turbine (T1) as a function of the relative position of the upstream turbine (T2), expressed as the change compared to free-flow conditions. The results show an asymmetric behaviour with respect to the cross-flow offset: fatigue loads are reduced when T2 is located at negative cross-flow offsets, i.e., when the wake impinges on the right side of the rotor of T1, while fatigue loads are increased for positive cross-flow offsets. A similar asymmetry has also been reported in previous work by Krathe et al. (2025) and Quick et al. (2025). The beneficial effects of wake impingement are not as strong as the detrimental effects. The reduction of fatigue loads reaches up to 6% (front bearing: 16 m/s) while the increase in fatigue loads reaches up to 26% (front bearing: 10 m/s). Smaller turbine spacing amplifies the effect for all wind speeds.

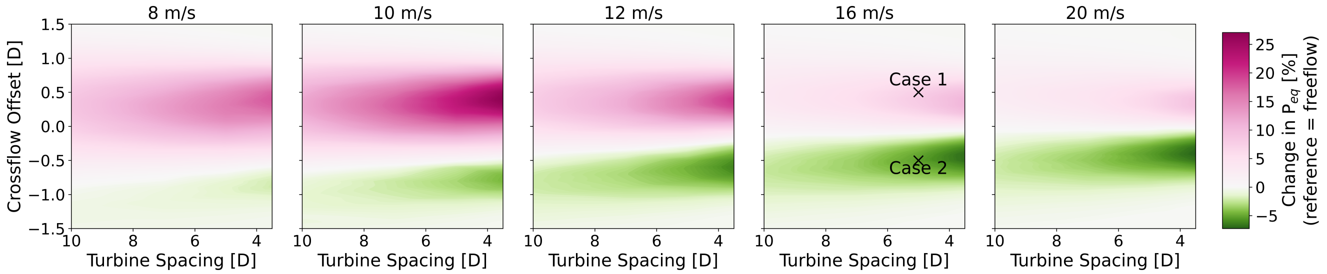

(a) Front bearing (non-locating)

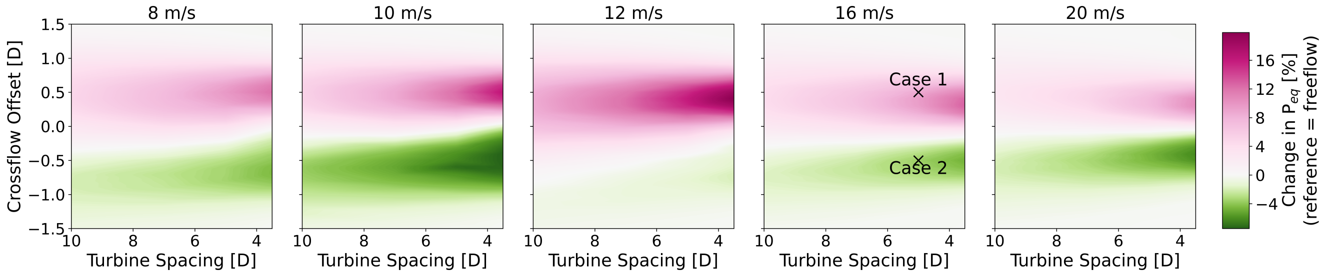

(b) Rear bearing (locating)

Figure 4. Fatigue loads in the main bearings of T1 as a function of the relative location of T2, expressed as the change in P_{eq} with reference to free-flow conditions.

To illustrate the mechanisms behind the asymmetry, two representative cases are introduced and compared to the free-flow reference case. The two chosen cases are marked in Figure 4 and the corresponding simulation setups are shown in Figure 5. The cases are:

- **Case 1**: Positive cross-flow offset (+0.7D) at 16 m/s wind speed, wake impingement on the, in wind direction, left side of the rotor.
- **Case 2**: Negative cross-flow offset (–0.7D) at 16 m/s wind speed, wake impingement on the, in wind direction, right side of the rotor.

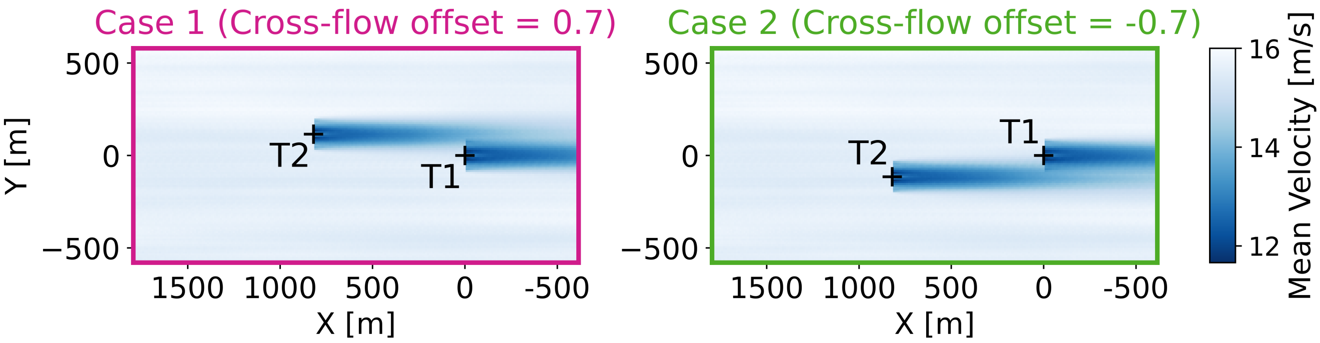

Figure 5. Simulation domain with turbine positions and time-averaged wind velocity for Case 1 and Case 2 at 16 m/s nominal wind speed, with a turbine spacing of 5D and cross-flow offsets of +/- 0.7 D.

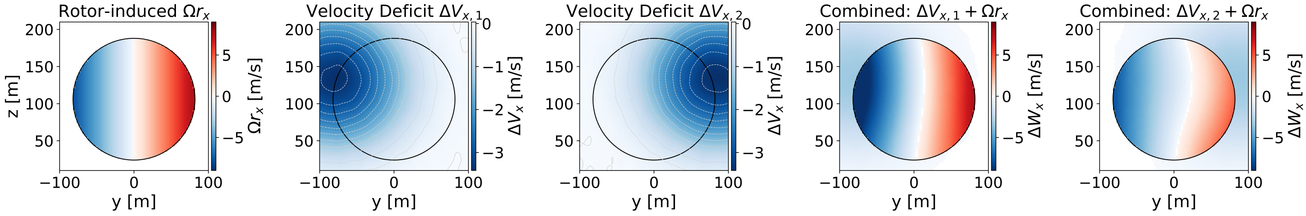

(a) (b) (c) (d) (e)

Figure 6. Change in relative velocity at the rotor blades due to wake deficit and shaft tilt

The differences in bearing loads between Case 1 and Case 2 are linked to the interaction of the wake deficit with an inherent aerodynamic asymmetry at the rotor, caused by shaft tilt. The asymmetric aerodynamic loading and the resulting yaw moment for wind turbines with a tilted shaft are described in detail by Hansen (1992) and Sandua-Fernández et al. (2023). Essentially, rotor rotation induces an in-plane velocity (Ωr) at the blade sections, which modifies the relative wind speed experienced by the blades (W). Because the rotor plane is tilted with respect to the incoming wind, part of Ωr projects onto the wind direction as a parallel component, denoted Ωr_x. Its values across the rotor disc can be described by:

$$\Omega r_x = (\Omega r \sin\psi)\sin\phi \tag{10}$$

where Ω is the rotor's angular velocity, r the radial location along a blade, ψ the azimuth angle, and ϕ the shaft tilt angle (Hansen, 1992). For this calculation, the blades are assumed to be rigid, the precone angle of the rotor is set to be 0 and the rotor speed to match rated operation (10.5 rpm).

As shown in Figure 6, for a clockwise-rotating rotor, Ωr_x opposes the inflow on the right side (ψ 0°–180°), thereby increasing the relative wind speed at the blades, W, while it aligns with the inflow on the left side (ψ 180°–360°), reducing W. This mechanism produces asymmetric aerodynamic loading across the rotor plane, even under homogeneous inflow.

For clarification, it should be noted that the velocity component of Ωr that is perpendicular to the wind direction also influences W. This effect, however, is largely homogeneous across the rotor disc. The existing non-homogeneities are symmetric on both sides of the rotor disc and negligible, compared to the influence of Ωr_x.

When the downstream turbine is partially impinged by the upstream wake, the local velocity deficits either amplify or mitigate the asymmetric aerodynamic loading. The wake-induced velocity deficits at the rotor of T1 are denoted $\Delta V_{x,1}$ for Case 1 and $\Delta V_{x,2}$ for Case 2 and are shown in Figure 6b and c, respectively.

Superimposing $\Delta V_{x,i}$ with the rotor-induced Ωr_x yields the change of the relative wind speed at the blades over the rotor area, denoted ΔW_x and shown in Figure 6d and e. In Case 1, the range of ΔW_x is larger as the wake-induced velocity deficit lies on the left rotor side, further increasing the pre-existing asymmetry. In Case 2, the velocity deficit lies on the right side, counteracting the rotor-induced velocity Ωr_x and thereby reducing the asymmetry.

To understand how the resulting changes in W affect the main bearing loads, the aerodynamic loads on the blades and the rotor must be examined. Figure 7 shows the blade and rotor loads for the two introduced cases and during free-flow conditions, as a function of the azimuth angle. The full rotation is averaged in 1° bins using data from 600s simulations.

Generally, as a blade experiences variations in W over a rotation, it will generate varying lift forces and loads depending on the azimuth angle. This is most prominent in the out-of-plane bending moments (Sandua-Fernández et al., 2023), shown in Figure 7a for a single blade. The resulting polar curves are not perfectly circular, reflecting the asymmetric aerodynamic loading. To highlight this non-circularity, Figure 7b shows the same curves after subtraction of the mean out-of-plane bending moment under free-flow conditions (11.7 MNm). The indentation between 180° and 220° stems from the tower damn effect, which results in a local reduction of wind speed and low bending moments on the blade (Santo et al., 2020).

Here, the crosses mark the centroid of each curve, which represents the net moment resulting from one full revolution of the blade. A centroid offset from the origin indicates an imbalance: vertical displacement corresponds to a net pitch moment, while horizontal displacement corresponds to a net yaw moment. Already under free-flow conditions, the centroid is eccentric, indicating nonzero pitch and yaw contributions. The pitch moment primarily arises from vertical wind shear, whereas the yaw moment originates from shaft tilt and the associated asymmetry in W_x. In Case 1, the horizontal offset of the centroid is more pronounced, consistent with the larger velocity differences across the rotor disk seen in Figure 6d. In Case 2, the centroid shows only a minor horizontal offset, indicating a small yaw moment, due to the smaller differences across the rotor disk seen in Figure 6e.

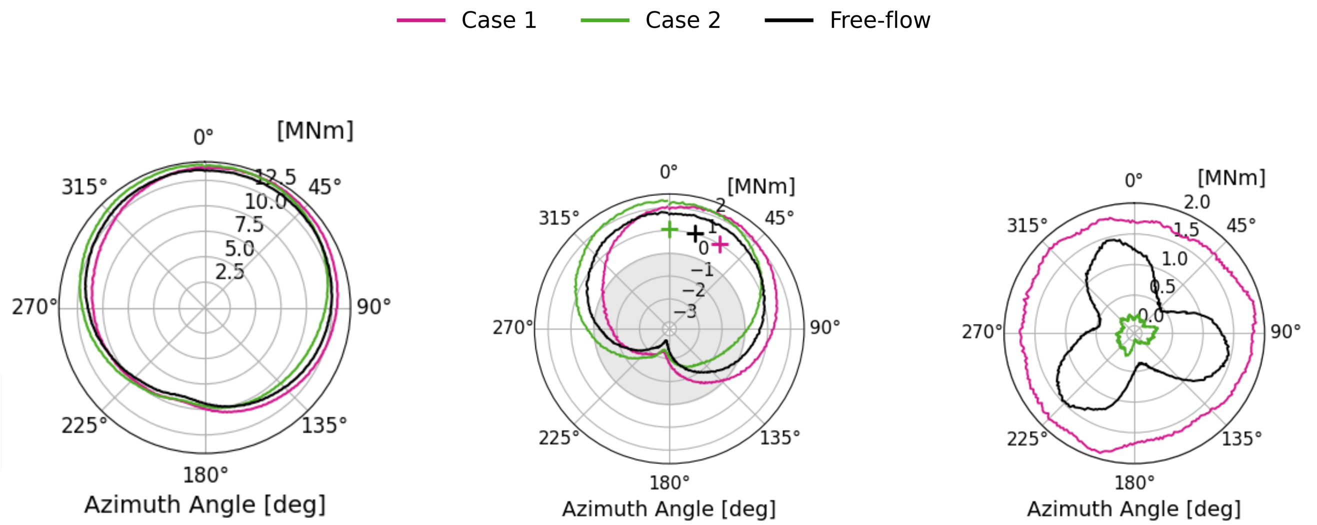

(a) Out-of-plane root bending moments for blade 1

(b) Out-of-plane root bending moments for blade 1 subtracted by mean value of free-flow conditions

(c) Yaw bending moments (M_z) at interface between hub and main shaft

Figure 7. Blade and rotor loads of Case 1, Case 2, and free-flow over the azimuth angle.

So far, only one blade has been considered; however, the same effect applies to all three blades. The combined contributions of all three blades yield a net yaw moment (M_z) at the interface between the main shaft and rotor hub, shown in Figure 7c. Consistent with the single-blade observations, Case 2 yields the lowest M_z (mean: 133 kNm), and Case 1 produces the highest (mean: 1746 kNm), while the free-flow case results in 948 kNm. Although the magnitude differs, the direction of M_z remains unchanged across all cases.

Finally, M_z is transmitted into the main bearings and results in the reaction forces described in equations 5 to 9, which determine the equivalent bearing load P_{eq} and the corresponding L_{10} lifetime. Since the front bearing carries exclusively radial loads, its P_{eq} is more sensitive to wake effects than that of the rear bearing, which also carries axial thrust.

The yaw bending moments were the main focus of this section, as they show the most apparent changes between cases. Other load components, such as pitch moments (M_y) and lateral forces, also contribute to P_{eq}, but their influence is less pronounced.

4 Case Study

The goal of the case study is to determine the impact of wake effects on the fatigue loads in a realistic wind farm layout, especially variations associated with wind direction and turbine positioning. For this, the layout of a wind farm in the Belgian North Sea is used. The farm consists of 28 8.4 MW turbines and has a total capacity of 235 MW.

The previously developed two-turbine simulation framework is extended to include all turbines in the wind farm. Their positions are defined based on the available GPS coordinates. The farm simulations are then carried out for three wind speeds (7, 10, and 14 m/s) and 16 wind directions, corresponding to wind-rose bins of 22.5°.

The load time series for every wind turbine are used to calculate the fatigue loads, as described in Section 2.2. To obtain reference values for the fatigue loads without wake impingement, additional simulations are performed for each turbine in free-flow conditions. The same wind fields are used between the full-farm and the reference simulations, and the locations of the individual turbines are kept consistent to maintain their relative positions with respect to the turbulence structures in the wind field. The fatigue loads between full-farm results and the reference values are then compared for each wind direction.

The results yield the relative change in fatigue loads at the blade root (DEL) and the main bearings (P_{eq}) as a function of wind direction for each turbine. Figure 8 presents exemplary results for turbine T2 at 10 m/s, while the position of T2 within the wind farm is found in Figure 10. The fatigue loads exhibit a high sensitivity to wind direction, with variations of up to 30% at the blade root and 17% at the main bearings. Consistent with the findings from the parametric study, wake impingement at the blade root leads exclusively to reduced fatigue loads, for instance at 337.5°, since the turbine operates below rated wind speed. In contrast, the main bearing loads increase for specific inflow directions (e.g., 225°) and decrease for others (e.g., 270°), with the increases generally outweighing the reductions. For wind directions between 67.5° and 202.5°, turbine T2 remains unaffected by wakes, as it is located at the boundary of the farm.

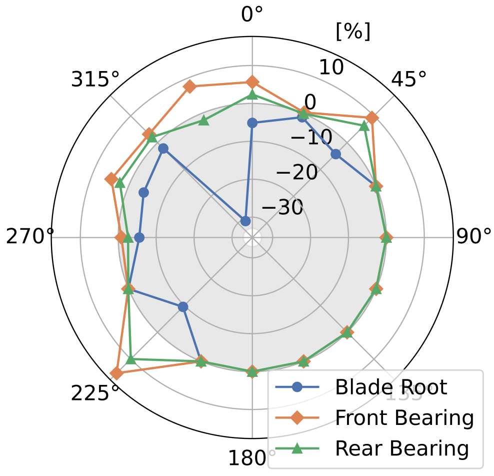

Figure 8. Change in fatigue loads of T2 w.r.t. free-flow conditions as a function of wind direction at 10 m/s.

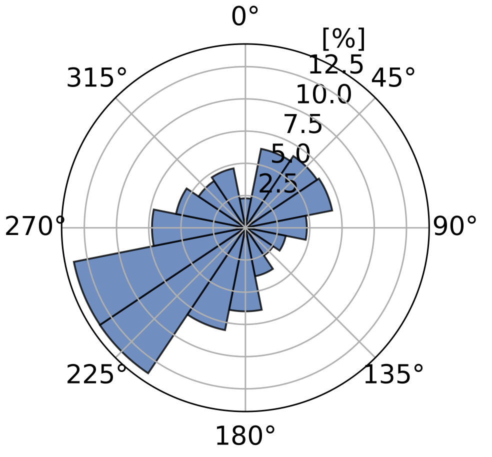

Figure 9. Occurrences of wind directions at 10 m/s wind speed.

To assess the farm-level impact of the directional fatigue loads, the simulation results are combined with the site-specific wind data. Based on 20 years of ERA5 data, occurrence frequencies are determined separately for wind directions of the three wind speeds. Figure 9 gives the occurrences of each wind direction for wind speeds between 9.5-10.5 m/s as a wind-rose. The occurrence frequencies are then applied as weighting factors to the directional fatigue loads. In this way, the resulting values of P_{eq} and DEL represent the expected fatigue loads for each turbine at a given wind speed, accounting for the site-specific distribution of wind directions. This metric is called the weighted fatigue load (WFL) and is calculated as:

$$WFL_T^{\text{Wind Speed}} = \sum_{d=1}^{N} w_d FL_{T,d} \tag{11}$$

Where T denotes the turbine index, d is the index of the wind direction bin, and N is the total number of bins (16). The term w_d represents the relative frequency of occurrence of wind direction bin d, such that $\sum_{d=1}^{N} w_d = 1$. Finally, $FL_{T,d}$ is the corresponding fatigue load metric (i.e. P_{eq} or DEL) of turbine T for wind direction bin d.

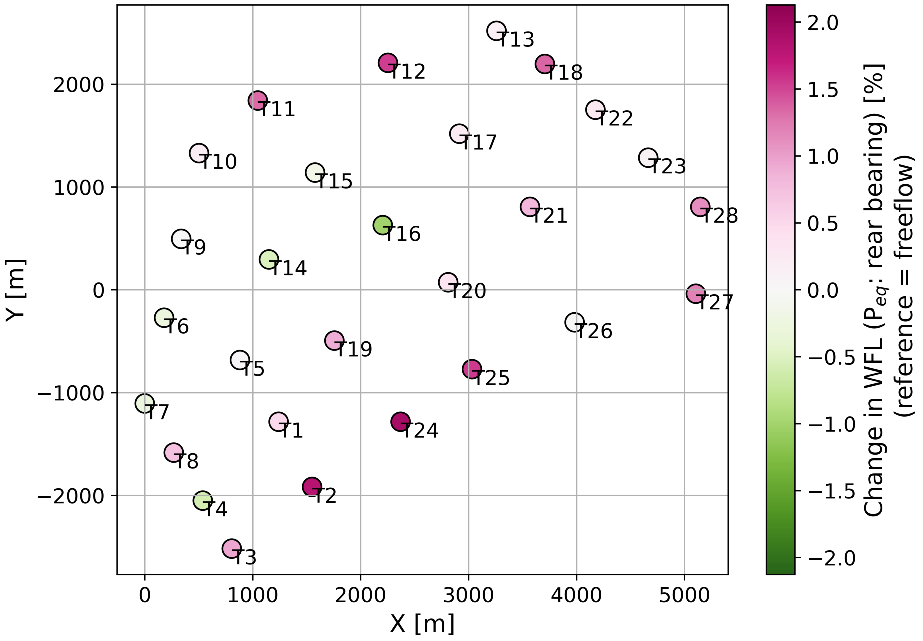

Figure 10. Changes in WFL of the rear bearings w.r.t. free-flow conditions, considering wind direction occurrences at 10 m/s wind speed.

Figure 10 shows the change in WFL for the rear bearing for all turbines in the farm, again expressed as relative changes with respect to conditions in case no other turbines are present.

The largest load increases (2%) are observed for turbines T2 and T24, which are exposed to wakes on the left rotor side under the prevailing south-westerly winds. In contrast, turbine T16 exhibits the most pronounced load reduction (1.1%), which can be attributed to wake interactions from turbines T5 and T14, resulting in impingement on the right rotor side under dominant wind directions.

https://doi.org/10.5194/wes-2026-13
Preprint. Discussion started: 26 January 2026

It should be noted that the relatively coarse directional binning of 22.5° may exaggerate extreme values. Taken Figure 8 as an example, the increase in bearing loads observed for turbine T2 at 225° is applied to the entire wind direction sector, even though the effect may in reality be confined to a much narrower range of inflow directions.

Figure 11a presents the aggregated results as a change in WFL compared to freeflow for all turbines and indicates the turbines with the minimum and maximum values. For below-rated conditions, the WFL for the blade root is reduced and has a large range, with the minima and maxima lying 10% points apart. For above-rated wind speeds, only T10 experiences a small reduction in fatigue loads while the remaining turbines experience increased fatigue loads with up to 6%.

For the main bearings, the mean result is an increase in fatigue loads, with an average of 2.3% for the front bearing and 1.3% for the rear bearing. The highest increase in fatigue loads is 5.3% at 10m/s for the front bearing and 5.8% at 14m/s for the rear bearing. Considering the equation for basic rating life of a bearing (Eq. 2) an increase of the fatigue loads (P_{eq}) by 5% results in a reduction of the endurable revolutions by 15%, i.e. a 15% shorter component lifetime, when assuming rolling contact fatigue is the limiting factor.

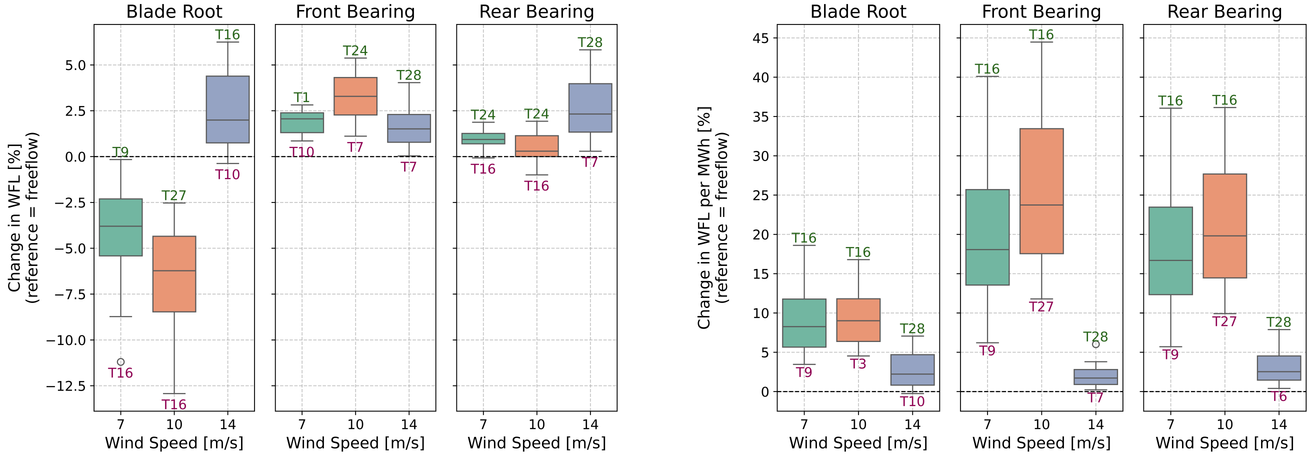

(a) Change in WFL

(b) Change in WFL per MWh of produced energy

Figure 11. Summary of the relative change in WFL for turbines in the wind farm in different wind speeds, with reference to free-flow conditions.

Figure 11b presents the same results normalised by the produced energy, expressed as changes in WFL per MWh. This representation highlights the impact of wake impingements on the fatigue-efficiency, i.e., the ratio between energy produced and fatigue damage accumulated by the component. A pronounced increase in fatigue loads per MWh is observed for all components under below-rated conditions. For example, main bearing fatigue loads per MWh rise by up to 43%, implying that the asset would generate only about 30% of the energy before failure compared to a turbine operating without wake effects. As the wind speed exceeds the rated value, this effect diminishes. Only strongly impinged turbines, where wake losses reduce the effective inflow below the rated speed of 11.4 m/s, still exhibit elevated fatigue loads per MWh. For below rated conditions, turbine T16 experiences the strongest changes in all metrics, followed by T1, T21 and T19, showing turbines to be less fatigue-efficient when located in the centre of the wind farm.

5 Conclusion

This work investigated the influence of wake impingement on the fatigue loads of offshore wind turbine components by conducting a controlled two-turbine parametric study and a case study of an operating offshore wind farm. The results consistently show that wake impingements substantially affect fatigue loading in both blade roots and main bearings.

In the parametric study, blade root fatigue loads were found to decrease (max. 30%) at wind speeds below rated due to the wake-induced velocity deficit, but to increase (max. 10%) at wind speeds above rated, in line with the thrust curve response. When power production is considered, the fatigue loads per unit of generated energy consistently rise under wake impingement, particularly in below-rated conditions where wake losses reduce power output and thereby reduce fatigue efficiency. Here an increase in DEL per MWh of up to 65% was observed.

The analysis of the main bearings revealed that fatigue loads were decreased (max. 6%) by wake impingements on the right rotor side, and increased (max. 26%) by wake impingements on the left rotor side. This asymmetry results from the interaction of wake-induced velocity deficits with the aerodynamic imbalance introduced by shaft tilt, which modulates yaw moments at the hub. These findings underscore the importance of accounting for shaft-tilt-induced asymmetries in drivetrain loading and indicate the potential of wake steering strategies to mitigate or exploit these effects. Increased turbine spacings are seen to reduce the influence of wake effects for both components, and the obtained results allow to weigh power density against increasing fatigue loads.

Extending the analysis to a real offshore wind farm demonstrated that fatigue loads are sensitive to wind direction and turbine position, such that the degradation rate of turbines varies within the farm. Factoring in the occurrences of wind directions, the fatigue loads in the blade root of the turbines were found to vary by up to 11% between turbines. In contrast, the fatigue loads of the main bearings differ by up to 5%, translating into significant lifetime differences. Turbines at the centre of the farm receive the greatest changes in the weighted fatigue loads compared to free-flow conditions. When normalised by produced energy, the results further showed that turbines subject to wakes become less fatigue-efficient, with main bearing fatigue loads per MWh rising by up to 43%.

The presented methodology demonstrates how a combined aeroelastic and farm-level simulation framework can quantify spatially varying turbine loading and translate it into component-specific fatigue loads. Such insights can support O&M strategies, guide remaining useful life assessments, and inform farm-life extensions. While the case study considered only three wind speeds, the framework is directly extensible to the full operational range, yielding a more comprehensive degradation map.

Extending this work should focus on two main directions. First, the analysis could benefit from finer directional binning and an extension to larger turbine clusters to better capture the sensitivity of wake interactions to the wind direction, as well as assess the severity of wake effects in larger offshore wind farms. Second, additional damage metrics can be incorporated to account for failure mechanisms beyond those covered by DEL and L_{10}. Examples that can be included without additional modelling steps are blade pitch bearing fatigue, as described by Rezaei et al. (2024), and tower bolt fatigue damage as described by Tao et al. (2024). Extending the framework with a multibody or a finite element approach will allow further fatigue metrics to be included in the analysis, such as those for drivetrain bearings and gears (Nejad et al., 2015) or for the support structure (Li et al., 2023).

6 Code availability

The code used in this study was developed in Python. The code can only be made available upon request to the authors, as it contains sensitive information.

7 Author contributions

Simulations were set up and carried out by JG and PJD, who also designed the methodology. Data was preprocessed and analysed by JG under the guidance of PJD, while DvB and VLK advised on wake dynamics and main bearing behaviour, respectively. The manuscript was prepared by JG, edited by PJD and DvB and reviewed by ARN and JH.

8 Competing interests

ARN is a member of the editorial board of the Wind Energy Science journal. The authors declare that they have no further conflicts of interest.

9 Acknowledgements

The authors acknowledge the Energy Transition Funds of the Belgian Federal Government for their funding of the BeFORECAST project and VLAIO (Flemish Agency for Innovation and Entrepreneurship) for the funding of the CORE project.

https://doi.org/10.5194/wes-2026-13
Preprint. Discussion started: 26 January 2026

References

Abbas, N. J., Zalkind, D. S., Pao, L., and Wright, A.: A reference open-source controller for fixed and floating offshore wind turbines, Wind Energy Science, 7, 53–73, 2022.

Barthelmie, R. J., Pryor, S. C., Frandsen, S. T., Hansen, K. S., Schepers, J., Rados, K., Schlez, W., Neubert, A., Jensen, L., and Neckelmann, S.: Quantifying the impact of wind turbine wakes on power output at offshore wind farms, Journal of Atmospheric and Oceanic Technology, 27, 1302–1317, 2010.

Binsbergen, D. W. v., Wang, S., and Nejad, A. R.: Effects of induction and wake steering control on power and drivetrain responses for 10 MW floating wind turbines in a wind farm, Journal of Physics: Conference Series, 1618, 022 044, https://doi.org/10.1088/1742-6596/1618/2/022044, 2020.

Bossanyi, E.: Combining induction control and wake steering for wind farm energy and fatigue loads optimisation, Journal of Physics: Conference Series, 1037, 032 011, https://doi.org/10.1088/1742-6596/1037/3/032011, 2018.

Damiani, R., Dana, S., Annoni, J., Fleming, P., Roadman, J., van Dam, J., and Dykes, K.: Assessment of wind turbine component loads under yaw-offset conditions, Wind Energy Science, 3, 173–189, https://doi.org/10.5194/wes-3-173-2018, 2018.

Dimitrov, N., Pedersen, M., and Hannesdóttir, Á.: An open-source Python-based tool for Mann turbulence generation with constraints and non-Gaussian capabilities, in: The Science of Making Torque from Wind (TORQUE 2024): Modeling and simulation technology, no. 5 in Journal of Physics: Conference Series, IOP Publishing, United Kingdom, https://doi.org/10.1088/1742-6596/2767/5/052058, 2024.

Fleming, P., Gebraad, P. M., Lee, S., van Wingerden, J.-W., Johnson, K., Churchfield, M., Michalakes, J., Spalart, P., and Moriarty, P.: Simulation comparison of wake mitigation control strategies for a two-turbine case: Simulation comparison of wake mitigation control strategies for a two-turbine case, Wind Energy, 18, 2135–2143, https://doi.org/10.1002/we.1810, 2014.

Freebury, G. and Musial, W.: Determining equivalent damage loading for full-scale wind turbine blade fatigue tests, in: 2000 ASME wind energy symposium, p. 50, 2000.

Gebel, J., Rezaei, A., Daems, P.-J., Marini, R., Matthys, J.-J., Nejad, A. R., and Helsen, J.: Wind turbine blade root and blade bearing fatigue damage estimation based on field data, Forschung im Ingenieurwesen, 89, 16, 2025a.

Gebel, J., Rezaei, A., Krathe, V. L., Vemuri, A., Daems, P.-J., Matthys, J. J., Sterckx, J., Vratsinis, K., Kestel, K., Nejad, A. R., and Helsen, J.: System identification of offshore wind turbines for model updating and design validation using field measurements (Preprint), Wind Energy Science, 2025b.

Hansen, A.: Yaw dynamics of horizontal axis wind turbines, Tech. rep., National Renewable Energy Lab.(NREL), Golden, CO (United States); Utah Univ . . . , 1992.

Hart, E., Clarke, B., Nicholas, G., Kazemi Amiri, A., Stirling, J., Carroll, J., Dwyer-Joyce, R., McDonald, A., and Long, H.: A review of wind turbine main bearings: design, operation, modelling, damage mechanisms and fault detection, Wind Energy Science, 5, 105–124, 2020.

IEC 61400-1: IEC 61400-1: Wind Energy Generation Systems – Part 1: Design Requirements, 2019.

IEC 61400-5: IEC 61400-5: Wind Energy Generation Systems - Part 5: Wind turbine blades, 2019.

ISO 281: ISO 281: Rolling Bearings – Dynamic Load Ratings and Rating Life, 2007.

Katsaprakakis, D. A., Papadakis, N., and Ntintakis, I.: A comprehensive analysis of wind turbine blade damage, Energies, 14, 5974, 2021.

Kecskemety, K. M. and McNamara, J. J.: Influence of wake effects and inflow turbulence on wind turbine loads, AIAA journal, 49, 2564–2576, 2011.

Keller, J., Sheng, S., Cotrell, J., and Greco, A.: Wind turbine drivetrain reliability collaborative workshop: a recap, Tech. rep., National Renewable Energy Lab.(NREL), Golden, CO (United States), 2016.

Krathe, V. L., Thedin, R., Jonkman, J. M., Nejad, A. R., and Bachynski-Polić, E. E.: Main bearing response in a waked 15-MW floating wind turbine in below-rated conditions, Forschung im Ingenieurwesen, 89, 37, 2025.

Larsen, G. C., Aagaard Madsen, H., and Bingöl, F.: Dynamic wake meandering modeling, 2007.

Li, B., Shi, H., Rong, K., Geng, W., and Wu, Y.: Fatigue life analysis of offshore wind turbine under the combined wind and wave loadings considering full-directional wind inflow, Ocean Engineering, 281, 114 719, 2023.

Liu, P. and Barlow, C. Y.: Wind turbine blade waste in 2050, Waste Management, 62, 229–240, 2017.

Meyers, J., Bottasso, C., Dykes, K., Fleming, P., Gebraad, P., Giebel, G., Göçmen, T., and van Wingerden, J.-W.: Wind farm flow control: prospects and challenges, Wind Energy Science, 7, 2271–2306, https://doi.org/10.5194/wes-7-2271-2022, 2022.

Mishnaevsky, L.: Root Causes and Mechanisms of Failure of Wind Turbine Blades: Overview, Materials, 15, https://doi.org/10.3390/ma15092959, 2022.

Nejad, A. R., Bachynski, E. E., Kvittem, M. I., Luan, C., Gao, Z., and Moan, T.: Stochastic dynamic load effect and fatigue damage analysis of drivetrains in land-based and TLP, spar and semi-submersible floating wind turbines, Marine Structures, 42, 137–153, 2015.

Nejad, A. R., Bachynski, E. E., and Moan, T.: On tower top axial acceleration and drivetrain responses in a spar-type floating wind turbine, in: ASME 2017 36th International Conference on Ocean, Offshore and Arctic Engineering-Volume 9: Offshore Geotechnics; Torgeir Moan Honoring Symposium, American Society of Mechanical Engineers (ASME), 2017.

OpenFAST Development Team: FAST.Farm Model Guidance, National Renewable Energy Laboratory (NREL), https://openfast.readthedocs.io/en/dev/source/user/fast.farm/ModelGuidance.html, accessed: 2025-05-27, 2024.

Porté-Agel, F., Bastankhah, M., and Shamsoddin, S.: Wind-Turbine and Wind-Farm Flows: A Review, Boundary-Layer Meteorology, 174, 1–59, https://doi.org/10.1007/s10546-019-00473-0, 2019.

Quick, J., Hart, E., Nilsen, M. B., Lund, R. S., Liew, J., Huang, P., Rethore, P.-E., Keller, J., Song, W., and Guo, Y.: Reductions in wind farm main bearing rating lives resulting from wake impingement, Wind Energy Science Discussions, 2025, 1–19, 2025.

Rezaei, A., Schleich, F., Menck, O., Grassmann, M., Bartschat, A., and Nejad, A. R.: Comparative analysis of rolling contact fatigue life in a wind turbine pitch bearing with different modeling approaches, in: Journal of Physics: Conference Series, vol. 2767, p. 052036, IOP Publishing, 2024.

Sandua-Fernández, I., Vittori, F., Martín-San-Román, R., Eguinoa, I., and Azcona-Armendáriz, J.: Platform yaw drift in upwind floating wind turbines with single-point-mooring system and its mitigation by individual pitch control, Wind Energy Science, 8, 277–288, 2023.

Santo, G., Peeters, M., Van Paepegem, W., and Degroote, J.: Effect of rotor–tower interaction, tilt angle, and yaw misalignment on the aeroelasticity of a large horizontal axis wind turbine with composite blades, Wind Energy, 23, 1578–1595, 2020.

Schaeffler Technologies AG & Co. KG: Bearing Catalogue: Large Size Bearings, Schaeffler Technologies, 2016.

Schmidt, F., Hübler, C., and Rolfes, R.: Kriging meta-models for damage equivalent load assessment of idling offshore wind turbines, Wind Energy Science Discussions, 2025, 1–30, 2025.

Shigley, J. E.: Shigley's Mechanical Engineering Design, McGraw-Hill, New York, 9th edn., 2011.

SKF Group: Rolling bearings—17000 Series (Catalogue), available via SKF MediaHub: Rollingbearings – 17000, 2018.

Tang, H., Lam, K.-M., Shum, K.-M., and Li, Y.: Wake effect of a horizontal axis wind turbine on the performance of a downstream turbine, Energies, 12, 2395, 2019.

Tao, T., Yang, Y., Yang, T., Liu, S., Guo, X., Wang, H., Liu, Z., Chen, W., Liang, C., Long, K., et al.: Time-domain fatigue damage assessment for wind turbine tower bolts under yaw optimization control at offshore wind farm, Ocean Engineering, 303, 117 706, 2024.

Thedin, R., Kreeft, J., Barter, G., Jonkman, J., and Shaler, K.: Impact of wake steering on loads of downstream wind turbines at an above-rated condition, Journal of Physics: Conference Series, 2767, 032 020, https://doi.org/10.1088/1742-6596/2767/3/032020, 2024. 445

Thomsen, K.: The statistical variation of wind turbine fatigue loads, 1998.